



Automatic Registration and Alignment on a Template of Cardiac Stress & Rest SPECT Images

Jérôme Declerck, Jacques Feldmar, Michael L. Goris, Fabienne Betting

► To cite this version:

Jérôme Declerck, Jacques Feldmar, Michael L. Goris, Fabienne Betting. Automatic Registration and Alignment on a Template of Cardiac Stress & Rest SPECT Images. RR-2770, INRIA. 1996. inria-00073922

HAL Id: inria-00073922

<https://hal.inria.fr/inria-00073922>

Submitted on 24 May 2006

HAL is a multi-disciplinary open access archive for the deposit and dissemination of scientific research documents, whether they are published or not. The documents may come from teaching and research institutions in France or abroad, or from public or private research centers.

L'archive ouverte pluridisciplinaire **HAL**, est destinée au dépôt et à la diffusion de documents scientifiques de niveau recherche, publiés ou non, émanant des établissements d'enseignement et de recherche français ou étrangers, des laboratoires publics ou privés.

***Automatic Registration and
Alignment on a Template of
Cardiac Stress & Rest SPECT Images***

Jérôme Declerck, Jacques Feldmar,
Michael L. Goris and Fabienne Betting

N° 2770

Janvier 1996

PROGRAMME 4



R ***apport
de recherche***

Automatic Registration and Alignment on a Template of Cardiac Stress & Rest SPECT Images

Jérôme Declerck*, Jacques Feldmar,
Michael L. Goris** and Fabienne Betting

Programme 4 — Robotique, image et vision
Projet Epidaure ***

Rapport de recherche n° 2770 — Janvier 1996 — 36 pages

Abstract:

Single photon emission computed tomography (SPECT) imaging is used to assess the location or the extent of myocardial infarction or ischemia.

A method is proposed to decrease the effect of operator variability and morphologically blind sampling in the quantification of scintigraphic myocardial perfusion studies. To this effect the patient's myocardial images (target cases) are registered automatically over a template image, utilizing non-rigid transformations. The registration method is an adaptation of the Iterative Closest Point algorithm.

Experiments have been lead on a database including 40 pairs of images selected to obtain a group of image abnormalities and variability. Upon the successful clinical validation of this work, a reliable, operator independent method for the analysis and interpretation of myocardial perfusion scintigraphies will be available.

Key-words: non-rigid matching, warping, medical image, SPECT, cardiology, 3D.

(Résumé : tsvp)

*E-mail: Jerome.Declerck@sophia.inria.fr

**Division of Nuclear Medicine, Stanford University Hospital, (Cal. USA)

***<http://www.inria.fr/Equipes/EPIDAURE-eng.html>

Méthode Automatique de Recalage et d'Alignement sur un Modèle d'Images Scintigraphiques Cardiaques Repos-Effort

Résumé :

La tomographie par émission monophotonique (SPECT, en anglais) au Thallium 201 ou au Technetium 99 est utilisée pour localiser et mesurer l'importance de zones ischémiées ou infarctées du muscle cardiaque.

Nous proposons une méthode pour réduire les effets négatifs de la subjectivité et de l'absence de considérations morphologiques dans les opérations de quantifications des images de perfusion myocardiques par scintigraphie obtenues lors d'examen cardiaques repos/effort. À cet effet, les images des patients sont recalées et alignées sur un modèle en utilisant des déformations non-rigides. La méthode utilisée est une adaptation de l'Algorithme du Point le Plus Proche Itératif.

Nous avons testé la méthode sur une base de données de 40 paires d'images sélectionnées pour obtenir une représentation large de variabilité et d'anormalités des images.

Sous réserve d'une validation clinique de ce travail, nous disposons d'une méthode qui permettra d'analyser et d'interpréter de façon objective (indépendante de l'opérateur) les images de perfusion myocardiques par scintigraphie.

Mots-clé : mise en correspondance non-rigide, déformation, image médicale, SPECT, cardiologie, 3D.

Introduction

Coronary artery disease remains one of the leading causes of death in the developed nations. In a large number of instances, the first symptom is due to a myocardial infarction, and half of the myocardial infarctions cause death. Detecting and preventing it is one of the major goals of modern medicine.

In the normal course of events, infarction follows a more or less progressive narrowing of the coronary artery. At first the narrowing does not interfere with resting blood flow, but, when during exercise the metabolic demands of the myocardium increase, the narrowed vessel cannot accommodate the required increase in blood flow. The myocardium, normally perfused at rest, becomes ischemic during stress or exercise (increased metabolic demand). This stress ischemia phase is the phase during which typical symptoms of coronary artery disease occur, and a period when the patient is both at risk for myocardial infarction, and when the disease is amenable to therapy. The classical symptoms are chest pain associated with exercise (typical angina) and changes in the EKG¹ during exercise. Sometimes the symptoms are less specific (or nearly absent!), and other conditions may mimic the symptoms. The defining diagnostic study is the coronary arteriogram, which reveals narrowing of the coronary arteries, and is needed for the planning and execution of the correcting vascular intervention (Coronary artery bypass graft or angioplasty). In view of the aspecificity of the symptoms, and the gravity of the potentially underlying condition, one is faced with the dilemma of performing too many unnecessary coronary arteriograms, and neglecting potentially lethal disease. For those cases in which the combination of risk factors, clinical signs and exercise EKG results are not sufficient to predict a high or low probability of coronary artery disease, an intermediate stratification step is necessary.

Nuclear medicine imaging provides 3D density maps of blood perfusion in a non-invasive way. In the stress-rest study, 2 perfusion maps of the heart muscle are taken: one obtained after an injection of the tracer at rest (rest image) and the other after the injection of the tracer during maximal exercise (stress image). Comparing the two images provides a classification of areas of the myocardium in 3 main classes (see Fig. 1):

- The intensity distribution is *normal* in both rest and stress images.
- There are one or more regions with abnormally low count rate densities in both the rest and stress image. The abnormality is fixed, and this connotes a myocardial *infarction*, or in some cases a very narrow stenosis, with resting hypoperfusion and a hibernating or stunned myocardium.
- There are one or more regions of low count rate densities in the stress image, but the densities are normal in the rest image. The abnormality is said to be transient, and connotes stress *ischemia*.

This encoding subsumes two comparisons: The patient's image is compared to a virtual image of what the normal distribution of densities should be (external comparison). This

¹electro-cardiogram



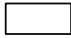
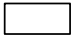

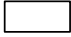
	Rest	Stress
Normal		
Infarcted		
Ischemic		

Figure 1: Classification of the perfusion of the myocardium from the nuclear medicine myocardial perfusion study. A filled square means a high intensity in the image.

virtual image accommodates normal variations. The stress image is also compared to the rest image (internal comparison).

The clinical examination in its current protocol stands in a "de visu" comparison of some central slices of the heart. This way of processing, with which the radiologists are used to working, has however three main drawbacks:

- the comparison is approximative, because of the lack of accuracy and the subjectivity of the "visual" matching of the two images of the heart,
- only central slices (taken from 3 different directions) are displayed and processed, excluding some intermediate areas (see Fig. 2),

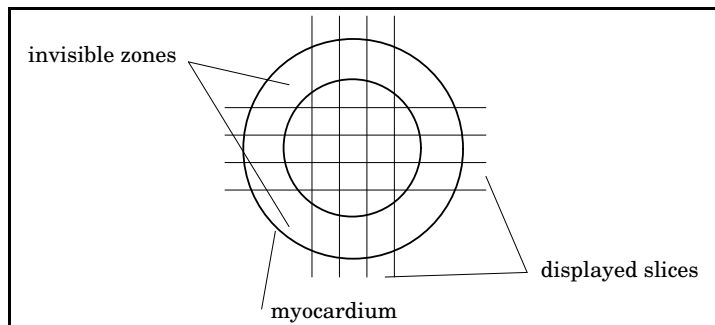


Figure 2: On this short axis slice, some areas of the left ventricle are not intersected by the displayed slices (vertical and horizontal lines).

- it is very hard to accurately compare different sets of images over time in order, for instance, to follow a specific disease or to check if a surgical intervention has been successful.

There is therefore a need to overcome the subjectivity of the visual comparison; various steps in the analysis (segmentation, orientation and centering, registration) have been automated in a variety of ways: works such as [15], [16], [7] define automatic methods to segment

the myocardium directly from the transaxial original images, or to define a center and a long axis [2]. Perault et al. [17], inspired from Woods et al. [27], find automatically a rigid registration between the stress and the rest image using correlation-based techniques. Venot et al. [25] use also a correlation-based technique with a stochastic sign change criterion to register the images. Slomka et al. [19] use also correlation techniques to find a non-uniform scaling transformation to register different hearts. A template is built by normalizing and averaging the resampled images. Some more complicated (free-form) transformations may be found with the method exposed in [21].

The aim of the method proposed in this paper is to provide a reproducible, robust and highly automatic way of comparing the stress and rest perfusion images of the same patient, or images of different patients. We introduce a robust 3D registration procedure, allowing in a further analysis a quantitative comparison of stress and rest images. We also introduce a registration with a “template” image of the heart, allowing a quantitative comparison with a model. The article is organized as follows: in the first section, the current clinical examination is exposed, detailing the different defects of the protocol, our method is explained in section 2 and detailed in sections 3 to 6 and in section 7, some results are discussed. We conclude by the perspectives of this work.

1 The Stress-Rest Clinical Examination

In this section, we explain the technical part of the clinical procedure, detailing when and how the images are taken, we also discuss the quality of the imaging technique (what is possible to be shown and the inherent defects) and the need of a stable quantification technique in order to obtain a reliable diagnosis.

1.1 SPECT images show a 3D perfusion map

1.1.1 The tracer

A radioactive tracer is injected into a peripheral vein. The tracer has two characteristics: Its distribution in the tissues is proportional to the distribution of tissue bloodflow, and clearance from the blood is rapid enough² so that most tissue accumulation occurs early. This phase is called *fixation*.

In some of the tracers the initial distribution slowly changes, until the distribution of the tracer reflects the the distribution pools or equilibrium distribution, rather than the flow distribution. This phase is called *redistribution* (see Fig. 3). Thallium 201 is known to redistribute in roughly 4 hours, but the Technetium 99 based tracers usually do not redistribute at all, or the redistribution time is much longer than the half-life of the radioactive isotope (6.02 hours for Technetium 99m, 73.5 hours for Thallium 201).

²a half-life of the order of two minutes

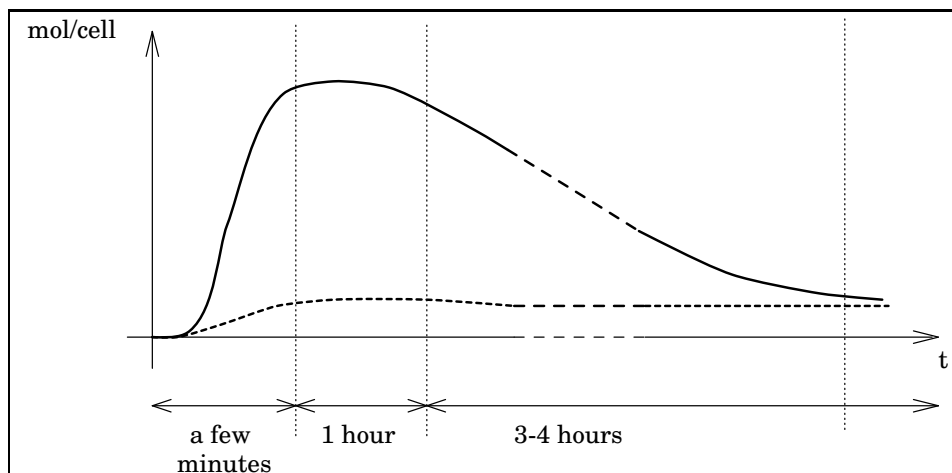


Figure 3: Evolution of the concentration of the Thallium 201 based tracer with time. After the injection, the tracer fixes in the cell in proportion of the blood flow, and redistributes as the flow distribution changes. The redistribution after an injection during a stress period lasts around 4 hours after a 1 hour long plateau. The continuous line show the evolution of the concentration for a normal muscle cell. The dotted line show the evolution of the concentration for a cell in an ischemic area at stress, where the tracer has not fixed much because of insufficient blood flow.

Measuring the amount of tracer in a particular volume indicates the relative level of perfusion of this volume during a relatively short time following the injection. This measure is processed by counting the β^- desintegrations of the radioactive label.

1.1.2 The clinical protocol

For the stress injection the patient is submitted to a physical exercise that increases the myocardial blood flow among other organ flows. The stronger the effort, the most important the need for blood, and hence, if any, the more obvious the perfusion defects. Exercise is continued until the hear rate reaches the maximum predicted heart rate (MPHR)³, or until significant EKG abnormalities appear, blood pressure fails to raise or falls, or the patients feels pain (angor) beyond a certain level. The injection is timed so that exercise will last two minutes after it, to maintain stress kinetics during the larger part of the tissue accumulation.

After the fixation ends and before the redistribution begins is the right time to take the 3D image of the perfusion distribution at stress. On Fig. 3, the first vertical line indicates the right time to take the stress image (just after the fixation is completed), the last vertical line show the time to take the redistribution image. The rest image is taken after the redistribution is completed or after a separate injection at rest.

³220 - the age of the patient beats per minute

1.2 Acquisition of scintigraphic images

1.2.1 The projection image, reconstruction

The distribution of the radioactivity within the patient is mapped in a number of projection images. They are taken at equally spaced angles, usually 32 projections over 180 degrees or 64 over 360. The typical size of the images is 64x64x64. The data are stored in a 64x64 matrix, with a pixel size of 5 mm x 5 mm.

Taking one projection takes around 10 seconds. During this shot, the patient is not asked to hold his breath, and of course, the heart does not stop beating. The image displays a heart in its *mean* position blurred by the beating and the breathing motions.

A three dimensional image is reconstructed from the projection data, usually by filtered back-projection. This reconstructed image is isometric, with a pixel size of 5 mm x 5 mm x 5mm.

1.2.2 Some manual processing

The reconstructed image includes the whole thorax of the patient. The heart is extracted as a subset of the original image. A rotation and a translation are manually performed in order to put the heart in a roughly standard position and direction (see Fig. 4 and Fig. 5).

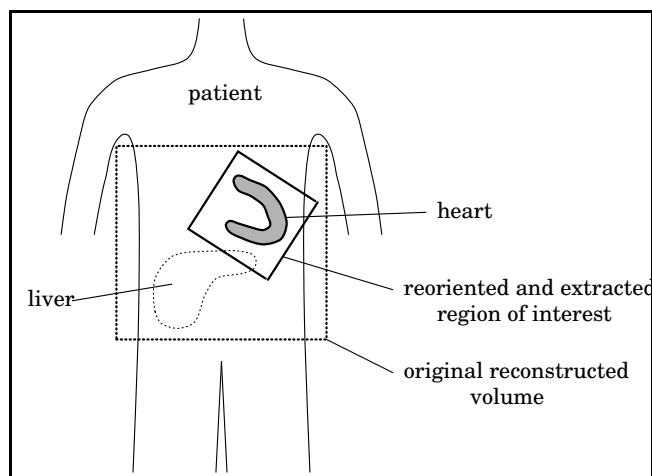


Figure 4: The heart is laying on the diaphragm. The small cube which defines the volume of the heart is extracted from the whole thorax transaxial image reconstructed from the projections. A part of the liver is often included in the extracted cube.

To avoid including other structures or organs such as the liver or the kidneys (which are very close to the heart and which fix easily the radioactive tracer), the image is masked through a manually designed shape.

The image is hence smoothed due to this extraction and resizing procedure. Usually, the rest image gives a better definition of the shape of the muscle than the stress image: as a matter of fact, ischemic zones appear as low intensity areas on the stress image, and

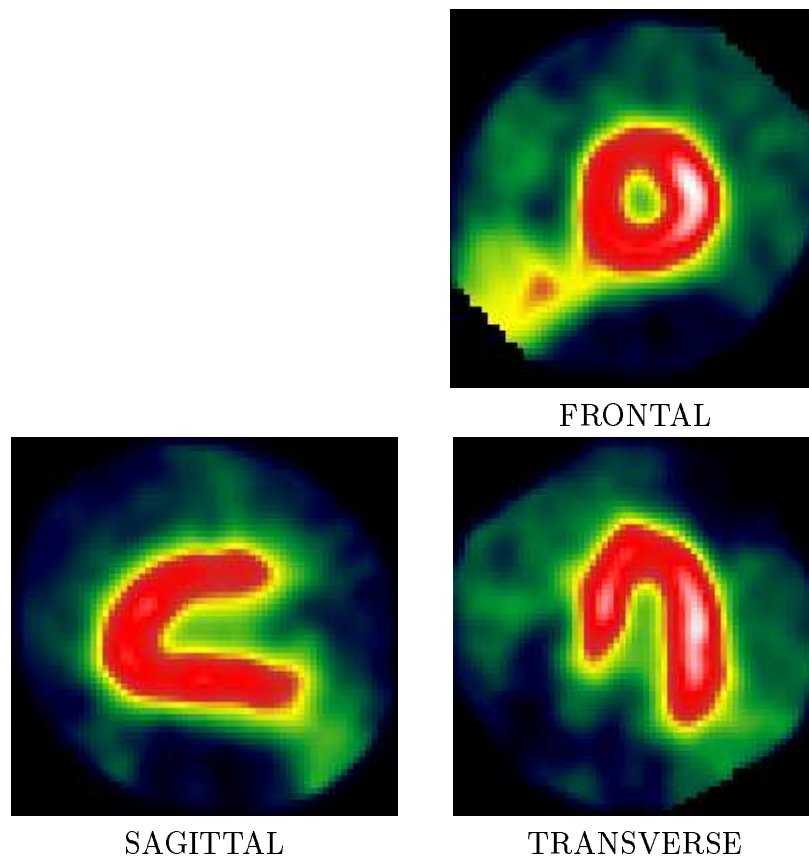


Figure 5: The reoriented heart: the slices show different views of the heart as it appears on conventional nuclear medicine interfaces. Bottom left on the frontal view, part of the liver appears beside the heart wall (infero-septal wall).

sometimes do not appear at all. The heart wall is thus more difficult to locate. The stress image however has a better contrast because there is less background noise and because the captation of the tracer is better in healthy regions: the contrast between ischemic and normal regions is due partly to a hypo-perfusion in ischemic regions and to a hyper-perfusion in healthy regions.

The tracer is either a molecule labeled with Technetium 99 or Thallium 201 as thallium chloride. The images produced with Technetium are usually of better quality because the energy of the emitted photon is higher (140 keV) than the ones emitted by Thallium disintegration (68-80 keV) and a higher dose can be injected.

1.3 Quantification of myocardial perfusion images

The quantification of scintigraphic myocardial perfusion images is generally based on some form of a polar transformation. In this approach the myocardial densities are sampled from an origin in the center of the cavity, along (evenly spaced) radii.

In one particular application [9] the three-dimensional images are sampled along rays or radii (radial sampling), originating in the center of the left ventricular cavity. Each radius is characterized by a longitudinal (a) and latitudinal angle (b). The origin of b is the apex, and b goes in 32 steps from 0 to 135 degrees, the origin of a is the middle of the lateral wall, and a varies from 0 to 360 degrees. A value sampled along the radius $R(a,b)$ is stored in the two-dimensional (64x64) vector (B) at the location (K,L) where K and L are defined as:

$$\begin{cases} K = \frac{32b}{135} \cos(a) - 32 \\ L = \frac{32b}{135} \sin(a) - 32 \end{cases} \quad (1)$$

The vector B is therefore a planar image in which central points represent apical locations, peripheral points represent the basal locations. The anterior wall is mapped on top, the inferior wall at the bottom, the septum in the left-hand side of the image (Fig. 6). This vector is comparable to the bull's eye maps described in the literature [5, 6, 12, 13, 23, 22, 24, 26], except for the fact that the distance from the center represents a latitude b in three dimensions, rather than a short axis plane position: The bull's eye map approach interrogates the volume as if it were a set of planes [8].

The effect of a polar transform amounts to a normalization of size and shape [10], since all morphological attributes of the image are reduced to angular coordinates (Fig. 7). This is also true for the polar component in bull's eye mapping, in which the third axis is divided in a set number of parallel "thick slices" between the apex and the base of the heart. This normalization allows the comparison between target cases and a population of normal cases, and the intercomparison of target cases.

There are four limitations inherent to this approach, of which two are alignment limitations [10]; one is due to the sampling direction and one is due to the inherent assumption that there is no relevant morphology except angular morphology.

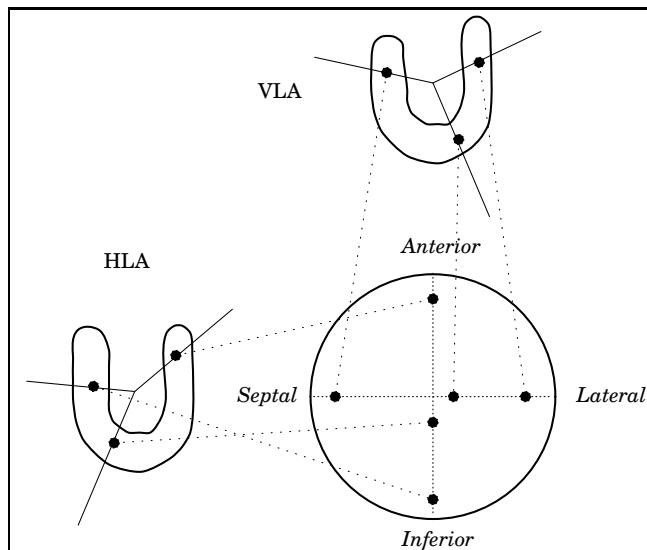


Figure 6: The figure shows the central horizontal and vertical long axis slices of a myocardium whose long axis is oriented north-south, with the apex pointing south. On each slice, a number of search radii are shown. The maximum count rate density is recorded along those radii and stored in the corresponding location on the polar map.

1. Alignment limitation: the effect of the origin location. Structures closer to the origin are relatively oversampled, and perfusion defects appear larger (Fig. 8-a).
2. Alignment limitation: angular shift. If the zero angle is misplaced identical distributions will appear different from each other (Fig. 8-b).
3. Sampling direction. If the lesion is relatively small and not well aligned in relation to the sampling ray direction, the lesion may be underdetected (Fig. 9-a).
4. Non-angular relevant morphology. The proportion of different parts of the myocardium are not necessarily fixed. The base of the heart, with the papillary muscles may be more or less prominent. Equal angular coordinates do therefore not necessarily map into identical myocardial structures (Fig. 9-b).

Alignment problems are mostly caused by operator variability in identifying the long axis and/or the center point, and attempts have been made to overcome this problem by using principal axis orientation [7]. It can be shown however that alignments based on the principal axes of simple geometric forms fitted to the myocardial surfaces does not guarantee stable center points relative to the organ or a stable anatomical alignment [19].

Sampling direction problems are only partially overcome by modifying the method by sampling in a direction orthogonal to the endocardial border tangent, where the sampling ray meets this border, since the direction of the defect across the myocardium is variable.

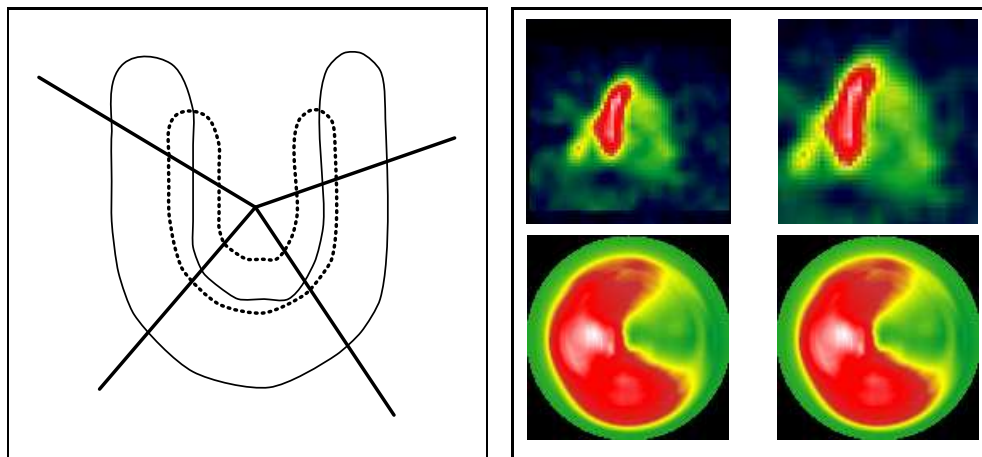


Figure 7: Implicit size normalization in polar or radial sampling.

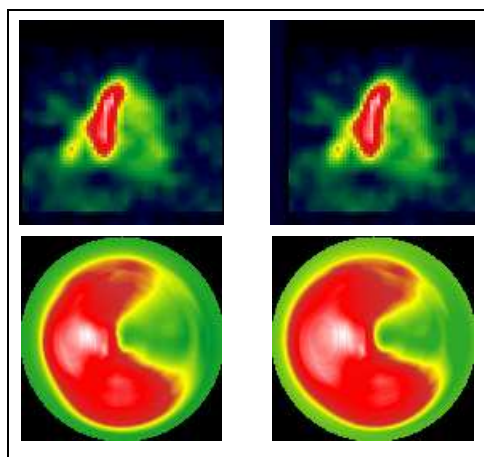


Figure 8-a
Effect of origin

The lateral defect appears smaller if the image is translated laterally (images on the right).

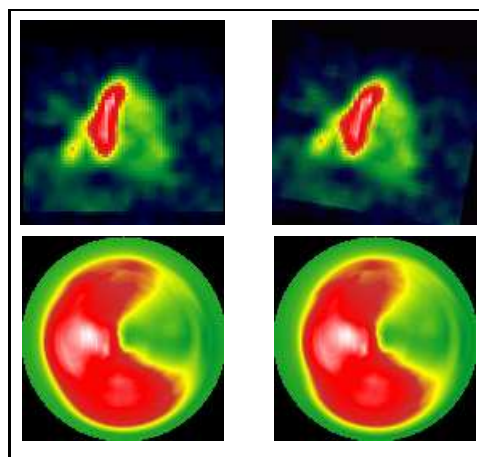


Figure 8-b
Angular mismatch

In this case, the same myocardial image has been slightly rotated, while maintaining the center. The polar maps differ.

Figure 8: Alignment limitations in mapping.

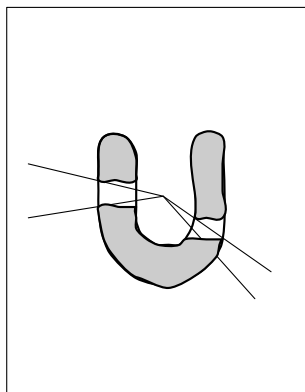


Figure 9-a

Effect of radial dir.

Depending on the direction of the defect, the sampling will include or exclude normal myocardium, underestimating the defect size.

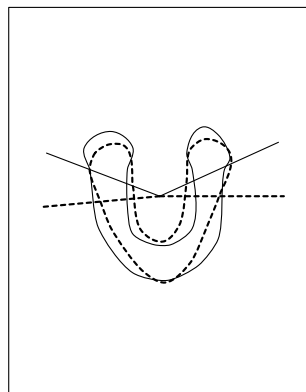


Figure 9-b

Unequal proportions

The angle at which the base thickening ends differs in two well aligned hearts.

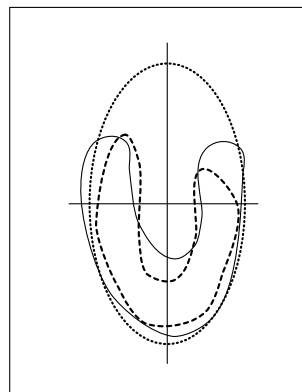


Figure 9-c

Principal axes method

Hearts sharing a common best fit ellipsoid are not aligned.

Figure 9: 3 different sampling direction problems.

A method is therefore needed which allows registration of target images automatically on a template image whose shape and size may be different, but with general morphological features which are similar. There are two results:

1. If this template is well oriented, the target image will be well oriented, and any small deviation from the ideal orientation will be constant across all target images.
2. Following the registration, predefined myocardial segments in the template image can be transferred exactly to the target image. As a result, size and shape normalization are obtained without the need for radial sampling, and regional count rate distributions can be compared from case to case.

2 Description of the method

Since the aim is to compare images between which major density distribution differences may occur, it appears logical to avoid matching algorithms based on density comparisons. The goal is indeed not to make densities equal, but to eliminate all size and shape difference while leaving density differences unperturbed. The methods we propose is therefore based on shape detectors based on gradients. One expects that gradients would exist even in low density areas. Second, the differences of sizes and shapes between different patients hearts do not allow to set easily a straightforward correspondence between an anatomically defined area and the coordinates (x,y,z) of a voxel in each 3D image (stress, rest, template).

The method that we propose splits has two major steps:

- The stress/rest pair of images is matched using a feature points based method, defining an affine transformation which gives a correspondence between a point in the stress image and a point in the rest image.
- A "template" heart is matched on the stress image using local spline transformations⁴ and both stress and rest images are resampled in its geometry.

After this transformation of the images (the output is a new stress/rest pair in a new geometry), the coordinates (x,y,z) of a 3D voxel in any image (stress, rest, template) correspond to the same part of the myocardium and allows quantitative intrapatient and interpatient comparison.

2.1 The matching step

In our method, each matching of two images is a 3 step process:

- automatic extraction of feature points in images 1 and 2, using a Canny-Deriche edge detector [14] in a particular geometry,
- matching of the two sets of points using an adaptation [4] of the iterative closest point method [1, 28]. This yields a 3D deformation function which transforms the point on image 1 to a point on image 2,
- resampling image 2 in the geometry of the image 1. Image 1 and the resampled image 2 are comparable pixel to pixel to measure perfusion differences.

2.2 Some further explanations about our choice

2.2.1 Two possible approaches

In an ideal situation where the matching with the model is perfectly performed against stress and rest images respectively, this provides for free the correspondence between the stress and rest images themselves.

In practice, any registration method (and especially 3D non-rigid ones) is error prone or at least an approximation of the ideal case. We therefore had to consider the following two possible strategies (Fig. 10):

1.
 - the stress and the rest image are separately matched on the template, producing two resampled images in the geometry of the template,
 - an a posteriori matching is performed with the 2 resampled images in order to correct the possible mismatches of the template registration.

⁴the local spline transformations are defined in section 4.4

- 2.
- the stress and the rest image are registered together,
 - the template is matched on one image (the stress image, for instance), and the pair is resampled in the geometry of the template.

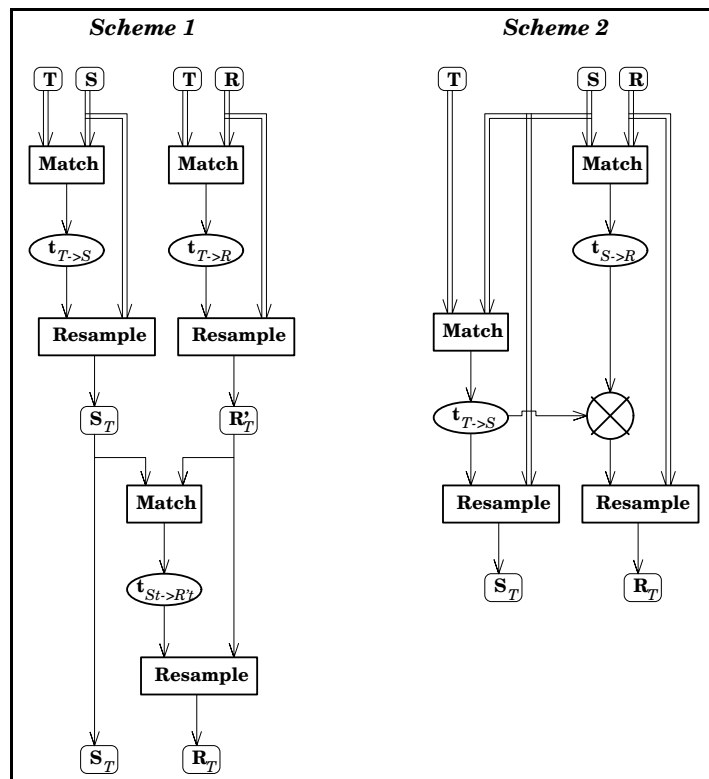


Figure 10: Two possible schemes for the registration method, R is the rest image, S is the stress, T is the template. R_T and S_T are the registered images resampled in the geometry of the template (the final output in both methods).

The reasons for choosing Scheme 2 instead of Scheme 1 are twofold:

- Scheme 1 is much complex and costly than Scheme 2 (3 matching steps versus 2), even if it is theoretically more satisfying and well balanced (between stress and rest).
- As soon as the stress/rest pair shows perfusion maps of the same heart, the geometry of the extracted feature points are similar (even if the intensity distribution is different). Matching the stress/rest pair is therefore easier than matching the stress image with the template for which the geometry of the feature points may strongly differ in size and shape. In terms of error accumulation, it is better to do the easiest step first and to end up with the more difficult.

2.2.2 The asymmetry of the process

Since the stress image is more likely to be incomplete (because of perfusion defects), it appears safer to match stress to rest rather than the rest to the stress.

3 Extraction of feature points

3.1 The images

Some characteristics of the scintigraphic images have to be taken into account:

- The densities do not necessarily match the anatomical features since perfusion defects may be present.
- There are high density areas due to the accumulation in other organs (especially the liver). Segmentation by thresholding only is unlikely to work in general.
- The noise due to the reconstruction from the 32 projections may be important.

3.2 Edge detection in a 3D polar map

The feature points we want to extract from the image are kind of edges of the heart wall. It would be useless to try to find a precise location of the true limit of the heart wall, because the image show only a heart in its mean position during acquisition and because spatial resolution is poor. The points we are looking for should be a rough but stable approximation of the myocardium edges.

To detect those feature points, we use an algorithm based on the first derivative of the image by detecting the edges with a Canny-Deriche recursive filter [14] in a particular geometry which is a kind of 3D polar map. The 3D polar map is defined as the original image resampled in spherical coordinates (r, θ, ϕ) (Fig. 11). From a 64x64x64 image, a 128x128x32 image is constructed.

The shape of a heart is roughly spherical around the apex and roughly cylindrical around the base. In the 3D polar map, this shape looks like a plate (Fig. 12).

Extracting edges in this map with a 3D edge detector provide a stable definition of gradient extrema points. Fig. 13 shows intensity profiles along 2 different radii starting from the center of the image.

Because of the mask sometimes used to hide non-cardiac areas, some artificial edges are created, with a very high gradient value (the background noise intensity decreases brutally from roughly 0.1 (normalized value) down to 0 in a one pixel shift). In order to eliminate such artificial extrema, the intensity profile along the radius is modified after the point before the last non-zero intensity point: intensity is set constant after this point⁵.

⁵The last non-zero intensity point has a biased value because of the resampling process: the intensity value of this point is corrupted by the vicinity of zero-intensity points.

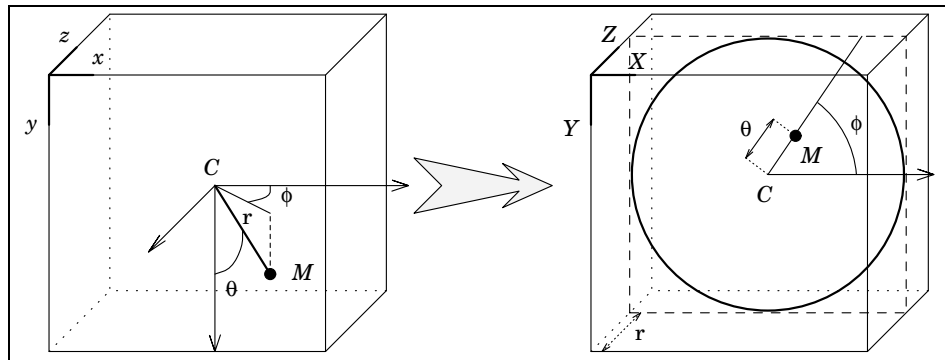


Figure 11: The (x,y,z) cartesian location of the black dot is converted into spherical coordinates in the 3D polar image, the depth Z is the distance from the center of the cartesian image, the position (X,Y) in the plane is defined with the two angles θ and ϕ , like in the 2D polar mapping.

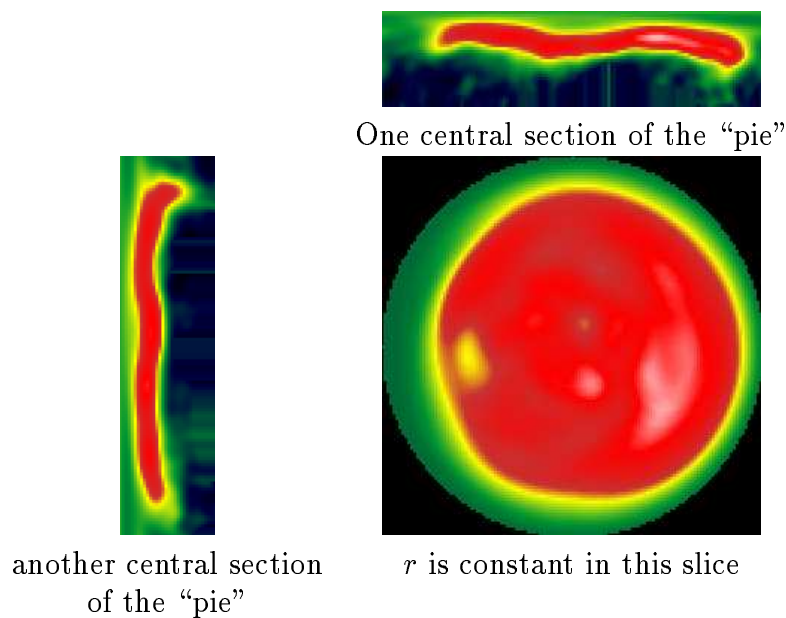


Figure 12: Some slices of the 3D polar map of the heart shown on Fig. 5. Because a heart roughly looks like a sphere, in this geometry, it looks like a “pie”.

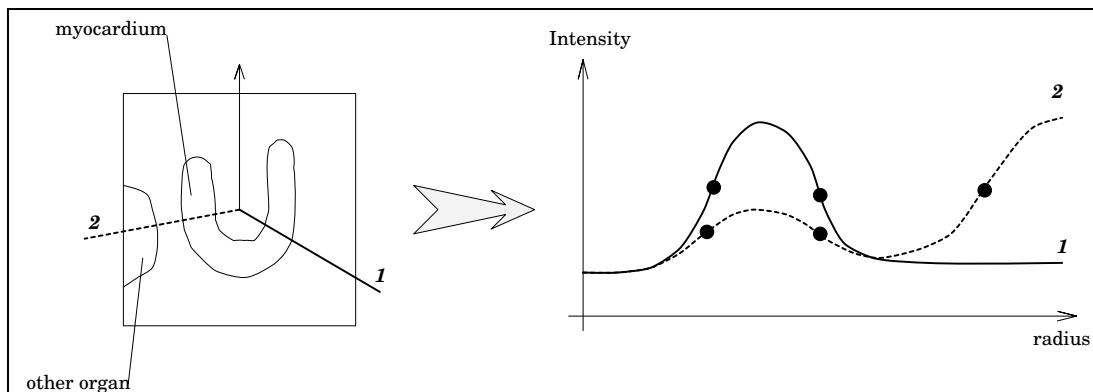


Figure 13: Intensity profiles along 2 different radii starting from the center of the image. The black dots show on both curves the edges detected with the Canny-Deriche filter.

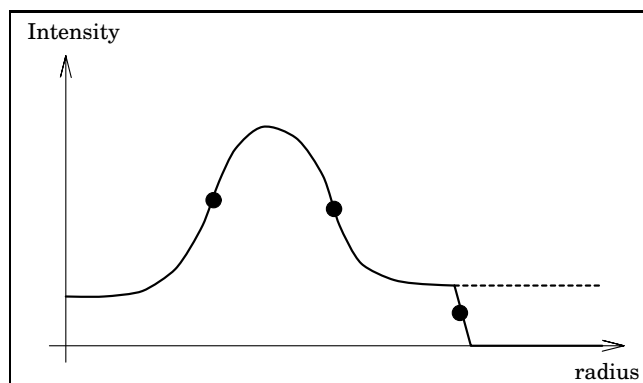


Figure 14: The original profile is shown of a solid line, the black dots show the detected edges. The third dot is an artificial edge due to a mask which brutally sets the intensity to zero. The dashed line shows the corrected profile used to remove this erroneous edge.

3.3 Filtering the edge points

Some detected edges do not correspond to the heart wall, as it is shown on the dotted curve on Fig. 13: an edge of another organ has been detected. Therefore, a last step is required: along a radius, on the intensity profile, the first *significant* increasing gradient extremum is likely to belong to the endocardium and the first following *significant* decreasing gradient extremum is likely to belong to the epicardium. Assuming this empirical description, we define some constraints to filter out a number of incorrect edge points:

1. any edge point in a 15 degrees cone around the apico-basal vector is eliminated. This angle value is very low, it is difficult to set correctly for a large database. Those points surely do not belong to the left ventricle.
2. a great majority of erroneous edge points are eliminated assuming that the filling procedure yields gradient extrema with constant gradient norm along a radius. Those extrema are detected on the deepest plane (32) of the polar map (a high radius value, for which we are sure that no cardiac structure is represented). If there is an edge point for $r = 32$, all the neighboring edge points which have the same gradient norm⁶ as this one are eliminated. Experiments on our database have shown that around 80 percent of those artificial edge points were removed.
3. the remaining points are sorted with respect to the absolute value of the Z coordinate of the gradient. A thresholding is performed on the contour image in order to eliminate the 20 lowest percent, and only large connected components are kept (minimum requested size is 500 points).
4. an ordering constraint is applied, we look for configurations fitting with our empirical description and reject edges for which we are sure they are non-cardiac: we reject every edge point after the first descending gradient extremum which is not too close to the center (a minimum radius of 5 is fixed as a threshold). On Fig. 15, different configurations of intensity profiles are listed with the corresponding algorithmic decision.

Finally, the points are converted back into cartesian coordinates. On Fig. 16, the result of feature extraction on different hearts. The proportion of good points is satisfying, the robust matching algorithm is able to cope with remaining outliers.

4 Robust matching

The edge detection is computed in both images (stress and rest, or stress and template). We assume that a first derivative extremum in the first image matches with a first derivative extremum in the second image. As soon as in the stress image, there may be less edge points

⁶tolerating a 0.1 margin due to the smoothing of the edge detection

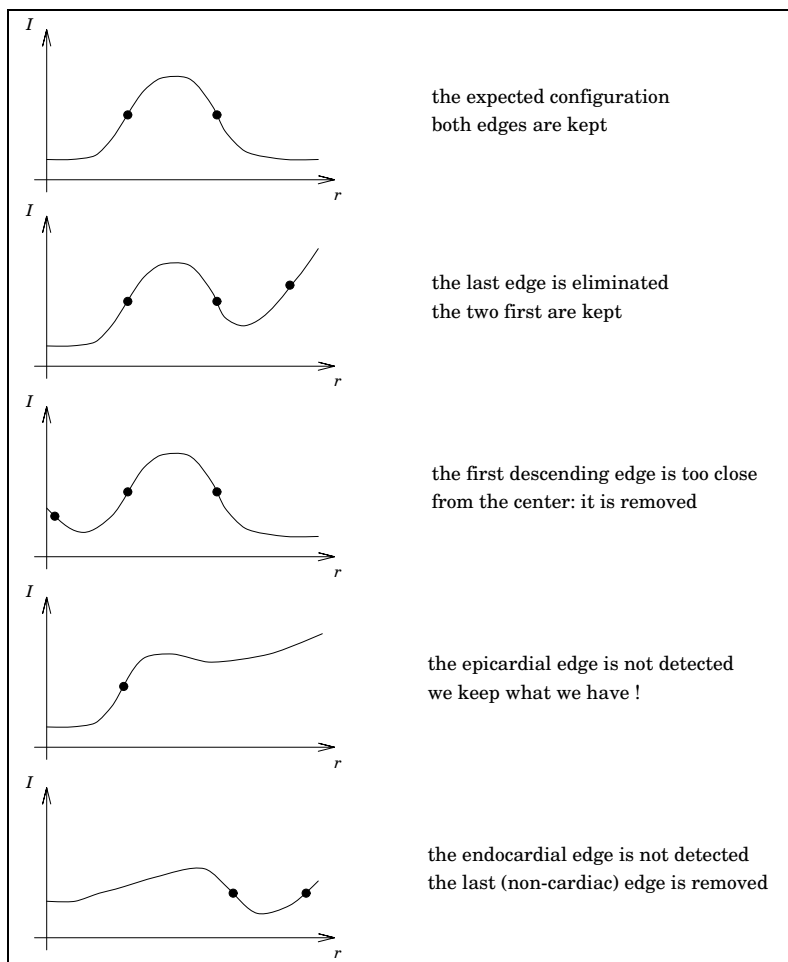
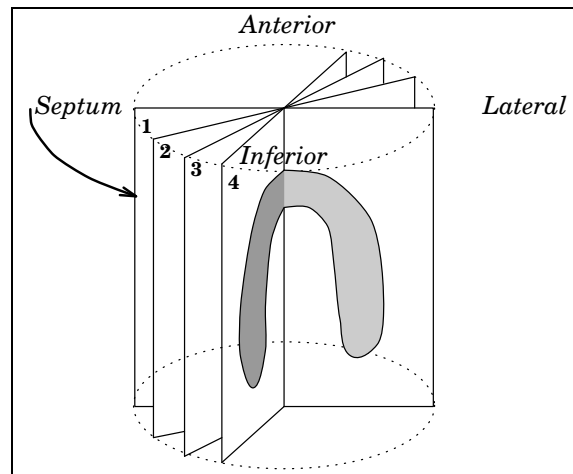


Figure 15: Left, some configurations for the intensity profile along a radius. Right, the consequent decision for the filtering.



septum on left, lateral on right lateral on left, septum on right
 inferior on left, anterior on right

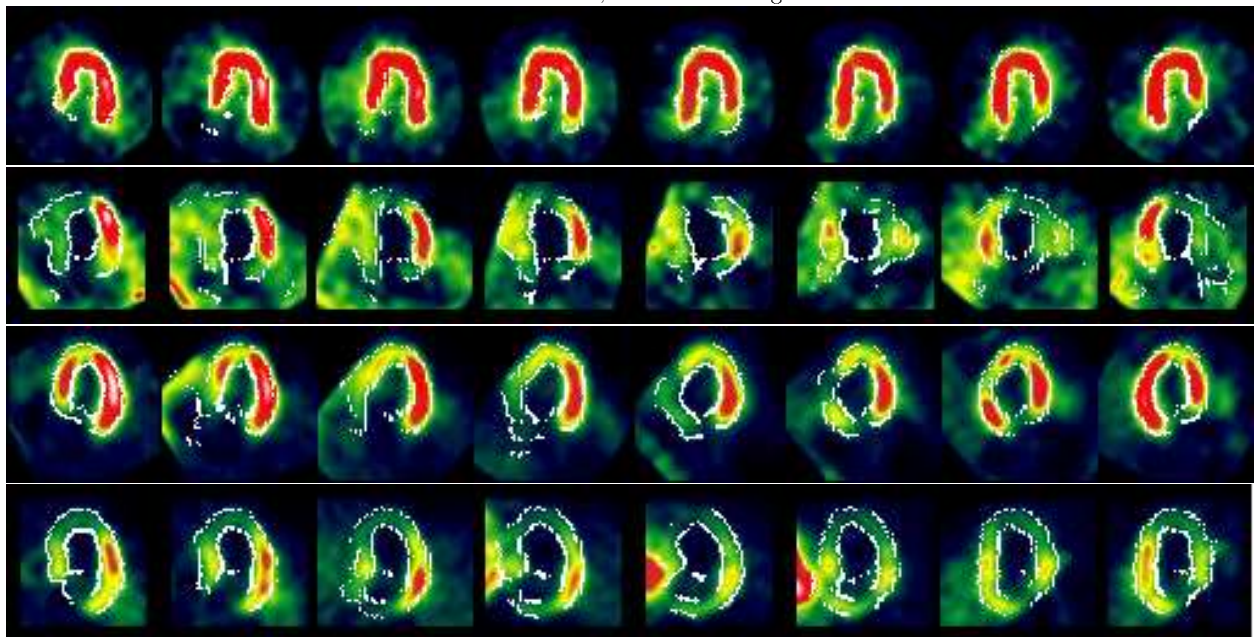


Figure 16: Edges (in white) automatically extracted and filtered from 4 different stress images (one patient per row). On each row, we see central slices resampled from the 3D image by rotation around the apex-base axis (see the representation on top drawing). This makes easier the display of the myocardial structure and avoids the problems of conventional displays (see fig. 2). We thus see how the method behaves with ischemic or infarcted areas (rows 2, 3 and 4).

than in the rest image, it is natural to try to find the transformation which deforms the stress edge points to the rest edge points.

The matching method is an enhancement of the iterative closest point [1, 28], adapted to our problem.

4.1 The matching criterion

Let us find a matching function F : given a 3D point M in Image 1, $F(M)$ should be the equivalent 3D point in Image 2. To calculate F , we assume that the image of a feature point in Image 1 is a feature point in Image 2. For the other points, an interpolation is made depending of the class of F . We define thus a criterion C :

$$C(F) = \sum_{M_i \in S_1} \|f(M_i) - \text{ClosestPointOnFP}_2(F(M_i))\|^2$$

Given a feature point in Image 1, the function F must give a point as close as possible to a feature point in Image 2 (this is what the function $\text{ClosestPointOnFP}_2$ calculates). The criterion is the sum of all residual distances extended to S_1 , a subset of the feature points in Image 1 for which the matching is considered as being reliable.

4.2 Minimizing the criterion

The minimization is an iterative process, given an initial transformation F_0 . This initial transformation is chosen in our experiments as the identity, assuming that the images to register are approximately well aligned. Each iteration n splits in three steps:

1. For each point M_i , we calculate $F_{n-1}(M_i)$ and we identify its closest feature point in Image 2. We therefore end up with a list of possible matched pairs of points.
2. We calculate the residual distance for each pair, and we decide whether a pair is reliable or not: we first eliminate the pairs for which the residual distance exceeds a fixed threshold. Second, we compute the mean μ and the standard deviation σ attached to the remaining pairs. We then eliminate the points for which the distance is superior to another threshold depending on the distance distribution ($\mu + c.\sigma$, where c can be easily set using a χ^2 table [4]). We get then for this iteration a list $S_{1,n}$ of reliable pairs of matched points. Notice that if a point is not matched in this iteration, it may be matched in a next one.
3. With the filtered list $S_{1,n}$ of pairs of points, we calculate F_n which is the best least square fit for the pairs of points. This new transformation is calculated within a class of acceptable functions (rigid, then affine and finally local spline).

The iterative process stops when a maximum number of iterations is reached, or when $S_{1,n} = S_{1,n-1}$. [4] gives further details about this adaptation of the iterative closest point algorithm, for instance about the convergence properties.

4.3 Definition of the closest point

The matching function $ClosestPointOnFP_2$ takes into account for each point its geometric position and the local direction of the intensity gradient calculated while extracting the edges. Considering 2 points M and N and their vectors \vec{n}_M and \vec{n}_N respectively, the distance between those 2 points is calculated as follows:

$$d(M, N)^2 = \alpha \|\overline{MN}\|^2 + \|\vec{n}_M - \vec{n}_N\|^2$$

where α is a ponderation coefficient.

This double definition of a point (location + direction) refines the matching criterion and makes it more robust in the presence of a crude initialization, for instance (Fig. 17).

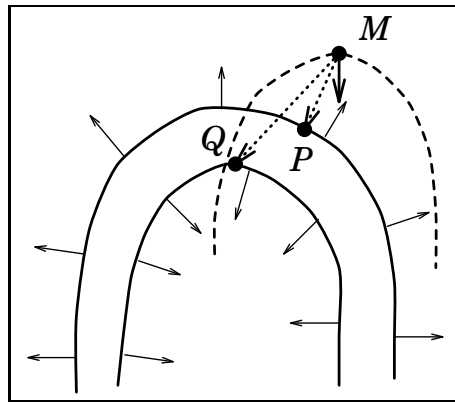


Figure 17: In dotted lines, the feature points of Image 2, in full lines, part of the feature points of Image 1. P is the closest point to M considering only geometric location, leading to a mismatch (endocardial point matched to an epicardial point). Q is the closest point to M taking into account the direction.

4.4 The class of transformations

The least square fit is calculated among a particular class of volumic transformations. We choose between:

- rigid (6 parameters define the transformation),
- affine (12 parameters define the transformation),
- local spline: the transformation F is a 3D tensor product of cubic B-splines. If we call (u, v, w) the coordinates of F :

$$u(x, y, z) = \sum_{i=0}^{n_x-1} \sum_{j=0}^{n_y-1} \sum_{k=0}^{n_z-1} u_{ijk} B_{i,K}^x(x) B_{j,K}^y(y) B_{k,K}^z(z)$$

$$v(x, y, z) = \sum_{i=0}^{n_x-1} \sum_{j=0}^{n_y-1} \sum_{k=0}^{n_z-1} v_{ijk} B_{i,K}^x(x) B_{j,K}^y(y) B_{k,K}^z(z)$$

$$w(x, y, z) = \sum_{i=0}^{n_x-1} \sum_{j=0}^{n_y-1} \sum_{k=0}^{n_z-1} w_{ijk} B_{i,K}^x(x) B_{j,K}^y(y) B_{k,K}^z(z)$$

with the following notations (for the x coordinate, for instance):

- n_x : the number of control points in the x direction. It controls the accuracy of the approximation (8 in our experiments).
- (u_{ijk}) : the 3D matrix of the control points abscissae. These are the parameters which define the transformation.
- $B_{i,K}^x$: the i^{th} B-spline basis function. Its order is K . These $B_{i,K}^x$ generate the vectorial space of piecewise K^{th} degree polynomials (see [18]). u is then a piecewise K^{th} degree polynomial in each variable x , y and z .

We choose cubic B-splines in our experiments ($K = 3$), because of their regularity properties. For the knots, we took the classic regular mesh:

$$\begin{aligned} t_0^x &= \dots = t_K^x = \min_x \\ t_i^x &= \min_x + (\max_x - \min_x) \frac{i - K}{n_x - K} \quad \text{for } K < i < n_x \\ t_{n_x}^x &= \dots = t_{n_x+K}^x = \max_x \end{aligned}$$

where \min_x and \max_x are the boundaries of the definition domain (the image domain).

In the definition of the criterion, a smoothing energy is added in order to control the regularity of the solution. This energy is expressed as a second order Tikhonov stabilizer:

$$SmoothingEnergy(u) = \int_{\mathbb{R}^3} \left[\frac{\partial^2 u^2}{\partial x^2} + \frac{\partial^2 u^2}{\partial y^2} + \frac{\partial^2 u^2}{\partial z^2} + \frac{\partial^2 u^2}{\partial x \partial y} + \frac{\partial^2 u^2}{\partial x \partial z} + \frac{\partial^2 u^2}{\partial y \partial z} \right]$$

and the same for the other coordinates y and z . This smoothing energy is ponderated by a coefficient in the global definition of the least square criterion. [3] gives a more complete description of the local spline transformation. The transformation is defined given a number of n_x, n_y, n_z parameters (= 512 in our experiments).

For our matching problems:

- Matching stress on rest: The shapes of the objects in both images are similar, some differences may appear in size but not very much in shape. We define F as an affine transformation. We apply first the algorithm with a rigid transformation in order to

have a good initialization and then with an affine transformation. The final result is the affine transformation F which best aligns the stress and rest images together. 10 iterations of rigid and 10 of affine are performed.

- Matching template on stress: The size and shapes of the objects are usually different, sometimes, a strong local deformation is necessary. We choose F as a local spline transformation. We apply first the algorithm with a rigid transformation, then with an affine transformation and finally with the local spline. The transformation thus gets more and more degrees of liberty in this progression (rigid, affine, local spline). 10 iterations of rigid, 10 of affine and 6 of local spline are performed. The criterion value is stable enough after these iterations so that we can consider that the process has converged.

5 Resampling the rest and stress images

After the matching step, we get a transformation from Image 1 to Image 2 $t_{1 \rightarrow 2}$. With this transformation, it is possible to build an image Image 2' which is the Image 2 resampled in the geometry of Image 1 (Fig. 18).

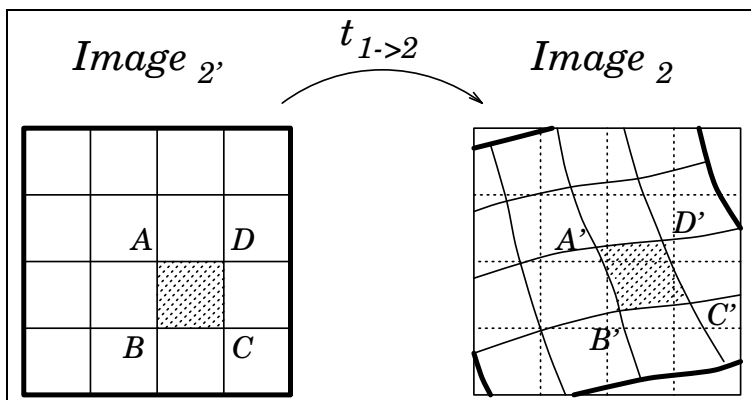


Figure 18: The resampling procedure is shown in 2D on this figure: the intensity of a pixel in Image 2' (the vertices of which are drawn as the square $(ABCD)$) is the integral of the intensity of Image 2 inside the area $(A'B'C'D')$, which is $(ABCD)$ deformed by $t_{1 \rightarrow 2}$.

Having computed the transformations $t_{T \rightarrow S}$ from the template geometry to the stress, and $t_{S \rightarrow R}$ from the stress geometry to the rest, it is possible to resample the stress image in the geometry of the template, and by composition ($t_{T \rightarrow R} = t_{S \rightarrow R} \circ t_{T \rightarrow S}$), we resample the rest image in geometry of the template after registration on the stress.

The resampling is a purely geometric transformation, the density counts information is not preserved.

6 Definition of the template

6.1 Our choice

To build the template of the heart, we adapt the previous segmentation process to an image of an average normal healthy heart, and we adapt the values of the parameters to obtain an almost perfect set of points (no gap on the heart wall, no spurious edge points outside the heart wall). We get then an almost ideal set of feature points.

In our experiments, the template is an image of one particular heart which is well defined and in good health (it is the heart of Fig. 5).

6.2 A definition of the volume of the LV

Our edge extraction method do not provide a structured set of points. To define the volume of the left ventricle, we used our matching method to deform an structured closed surface on our set of feature points. We take an isosurface as the closed surface: because the deformation is smooth, the structure of the surface is conserved.

This definition of the volume has to be validated, of course we are not sure to define the true boundary of the ventricle, because this information is not available from scintigraphic images. As for our method, this definition needs a clinical validation which will demonstrate whether or not it gives better segregation between normal and abnormal than classical definitions of the volume of the left ventricle.

6.3 Possible improvements

Slomka et al. [19] define a template as an average heart among a set of similar hearts after a correlation based matching with a non-uniform scaling transformation. We are currently working on a more sophisticated definition of our template(s ?) or model image which could conduct to statistical analysis and classification.

7 Results and discussion

7.1 The experimentation on the database

A set of 32 paired stress and rest images has been selected among the studies provided at the Department of Nuclear Medicine of the Stanford University Hospital (California, USA). Those images were selected to obtain a mixed group of image abnormalities and variabilities, with a more important proportion of “difficult” cases than an average database should contain in order to test the robustness of the registration algorithm. The method and the parameters have been set with this database.

Another 8 cases (chosen for their disparity in size and shapes) have been added to the database to make a crude validation of the parameters. A more extensive validation will be

processed with a routine database (the studies will not be selected on clinical or pathological characteristics). Our comments on this paper will be limited to morphological and perfusion considerations; quantification and stratification aspects will be discussed in a next paper.

The images were taken with both Tl 201 and Tc 99m tracers and prealigned manually by an expert (one of the authors: M. L. Goris). This alignment ensures that the center of the image is inside the cavity of the left ventricle and that the \vec{y} direction in the image is parallel to the apico-basal vector. Those constraints are crucial for our edge extraction step and they are not hard to satisfy.

7.2 The results

Fig. 19 shows the central frontal slices of the stress and rest images before and after registration and alignment. Each line shows a different patient from our database. The coded name of these patients are written on the left. Some more slices of the 3D images are shown for two different patients (RIDOMPA and RYALMPA on fig. 20 and 21 respectively). To validate the matching, we must be very careful about the definition of *what* the myocardium *is*. Using a colormap such as the one which we use to show the images⁷, we are conditioned to define the sane myocardium as the red and white part of the image inside the “yellow” isocontour boundary, which is not the definition we have adopted. We do not intend to define the true anatomical edges of the myocardium (this information is not really available from nuclear medicine images), but we define points for which we assume that they feature comparable characteristics from one image to another. That is why the points inlaid in white on fig. 19, 20 and 21 do not necessarily match with the “yellow isocontour” that the colormap defines.

On the slices (which are only a 2D abstracts of a 3D perfusion map), we can appreciate on the left two columns (the original rest and stress images) the differences in sizes and shapes of the patient hearts. On the next two columns, the morphological differences are removed whereas the perfusion information (the intensity level) is conserved.

On fig. 21 we can visually appreciate the robustness of the extraction of the edge points in the stress image of patient RYALMPA. This patient seems to suffer from a large anterolateral ischemia, which is revealed by the difference of intensity in that region between stress and rest images. Despite the intensity in the ischemic area is low (but not as low as the background noise), it has been possible to detect the cardiac edges.

As far as an expert can appreciate the result of the matching, for 80 % of the treated cases give satisfying results: in those cases, the feature points of the template deformed with the matching transformation define a plausible boundary for the left ventricle to an expert eye. For the last 20 % (which are difficult cases, according to an expert), some parts of the ventricle are not included in the volume or some non-cardiac areas are included in the volume. It appears that these errors are due, first, to some defects in the segmentation (the basis is not well defined, as for patient LEDOMPA, fig. 19) and second, because the local spline function does not deform enough. Improving the extraction of feature points

⁷from high intensities to lower ones, the color changes to white, red, yellow, green, blue and then black. This colormap is used on many usual nuclear medicine interfaces.

will give a major enhancement to the quality of the results; we are currently working on this particular subject.

Fig. 22 shows the surface of the template. This surface has been obtained by deforming an isosurface of the template to the feature points with our method. This closed surface can be a definition of the volume of the left ventricle. Fig. 23 shows 4 different hearts at stress (LOJUMPA, MCWAMPA, RIDOMPA and RYALMPA⁸) in 2 different projections. These surfaces were obtained by deforming the surface of the template with the deformation computed to match the template on the stress image. Some slices of those images are displayed on fig. 19, 20 and 21. With this method, it is possible to define a **volume of the left ventricle for any SPECT heart image**, which is a key-point in cardiac SPECT image quantification and analysis.

On fig. 23, the right column shows a regular 3D grid deformed by the alignment transformations of the 4 same hearts. The size of the grid is 10x10x10 and covers the whole image. The non-rigid deformation looks regular over the volume of the image.

The average time of the whole treatment (edge extractions + matchings + resamplings) is roughly 5 minutes per patient on a DEC Alpha workstation. We are currently working on some optimizations of the source code which could at least reduce the computational time by 50 %.

8 Conclusion

We presented in this article a highly automated method to register and align images from myocardial perfusion SPECT studies. To reconstruct “better” images, feature points are extracted in stress and rest images, the stress and rest points are matched together using an affine transformation (this gives the stress-rest registration) and the stress points are matched with a template using a local spline transformation (which gives the alignment). New images are resampled in the geometry of the template.

The method has been tested and implemented on a database of 32 stress-rest studies specifically selected to obtain a sample of image variability and abnormalities. An additional set of 8 cases was used to check the parameters, giving a first appreciation of the validation of the method.

In the future, we will define a clinical validation protocol of the process which will include an experimentation of the method on a large cohort of patients. The method will be validated by demonstrating that after polar sampling, the standard deviation around the mean of the normal case stress polar maps is smaller when this registration method is used, than if the alignment is performed by an experienced operator or the alignment which was performed in routine clinical practice prior to the design of this study. In addition, the method will be validated if, while the normal values are clustered closer around the mean, the abnormal cases remain distinct from the normal cases (that is if the reduction of normal variation does not result in the reduction of the difference between normal and abnormal).

⁸the last three cases belong to the 8 additional studies of the database.

After having validated the method, in a second step, we will work on an enhancement of the segmentation step and on a more sophisticated definition of the template. We will also work on a statistical analysis of the quantification of SPECT myocardial images, inspired by the works of Houston et al. [11] or Strother et al. [20] about the Principal Components Analysis.

9 Acknowledgements

We want to thank Focus Medical for their help in making the collaboration between the INRIA and the Stanford teams possible. The Focus team in Grenoble is currently working on the first steps of the industrialization of the method.

We give also special thanks to Grégoire Malandain, to the teams of the Stanford University Hospital (California, USA) and of the Centre Antoine Lacassagne (Nice, France) for the rich and constructive discussions and comments about the project.

This work was partially supported by regional grant of the Région Provence Alpes Côte d'Azur (doctoral research contract).

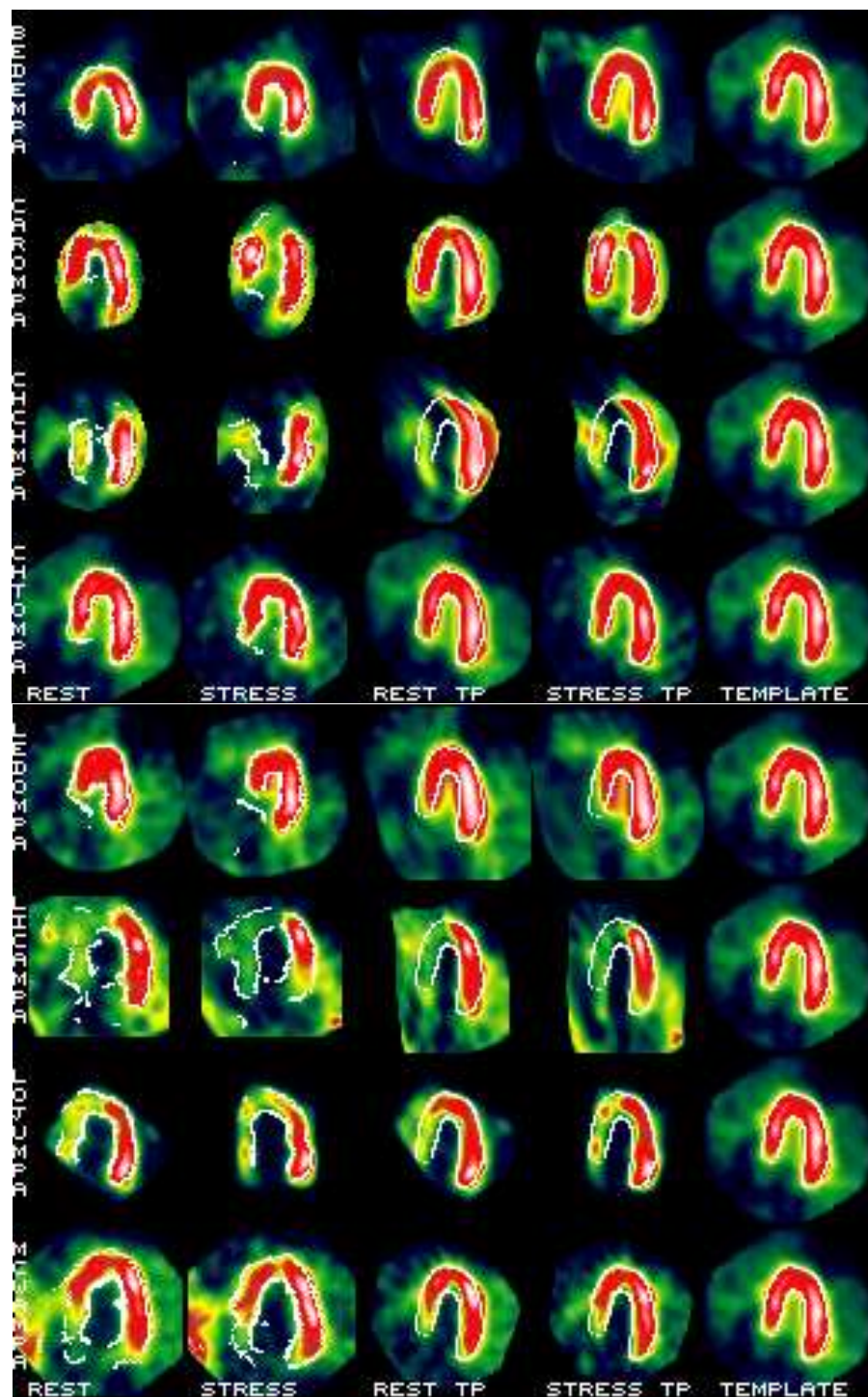


Figure 19: Experiments conducted on the database (I). Each row shows a different study (whose coded name is written on the left). Left two columns show central slices of the rest and stress images before registration. The detected edge points are inlaid in white. The next two columns on the right show the rest and stress images after registration and alignment. On the right column, the central slice of the template. The edge points of the template are inlaid in the images of the right three columns.

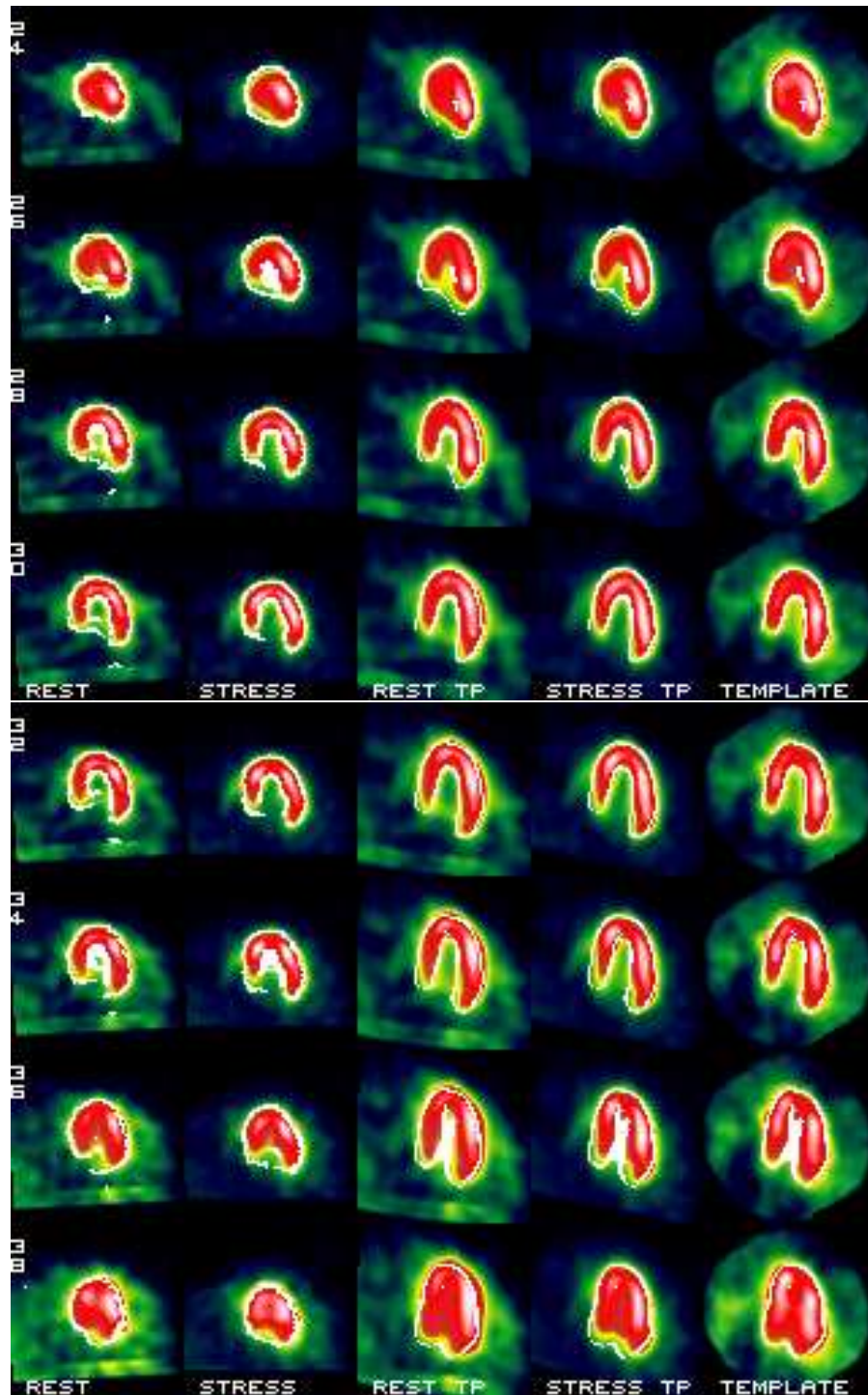


Figure 20: Experiments conducted on the database (II). Different transverse slices of patient RIDOMPA study. Left two columns show different transverse slices of the rest and stress images before registration. The detected edge points are inlaid in white. The next two columns on the right show the rest and stress images after registration and alignment. On the right column, the corresponding slices of the template. The edge points of the template are inlaid in the images of the right three columns.

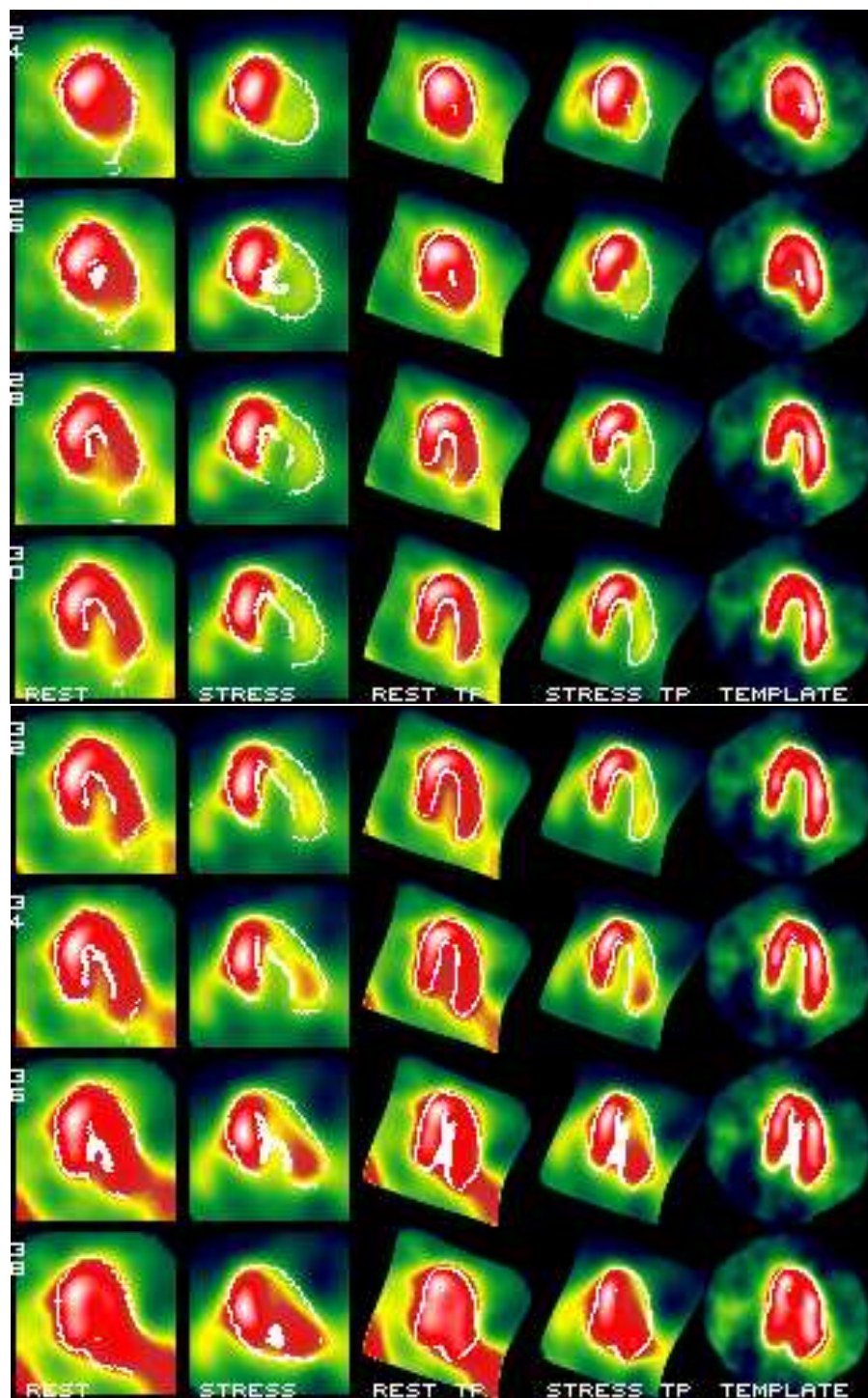


Figure 21: Experiments conducted on the database (III). Different transverse slices of patient RYALMPA study.

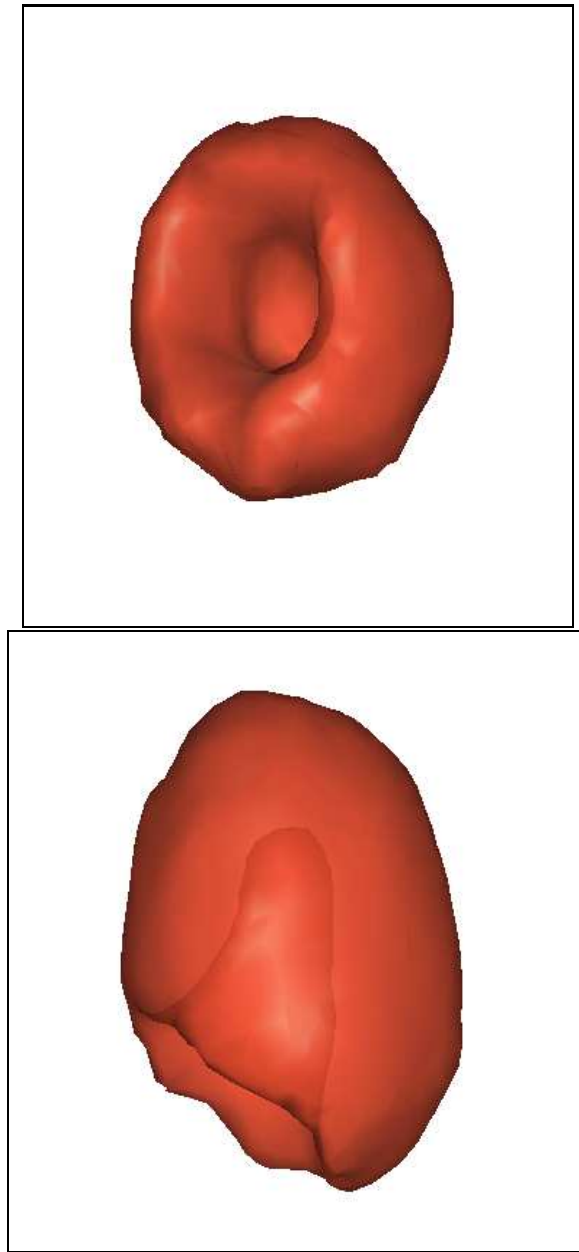


Figure 22: The closed surface of the template, top on a coronal projection and bottom on a frontal projection.

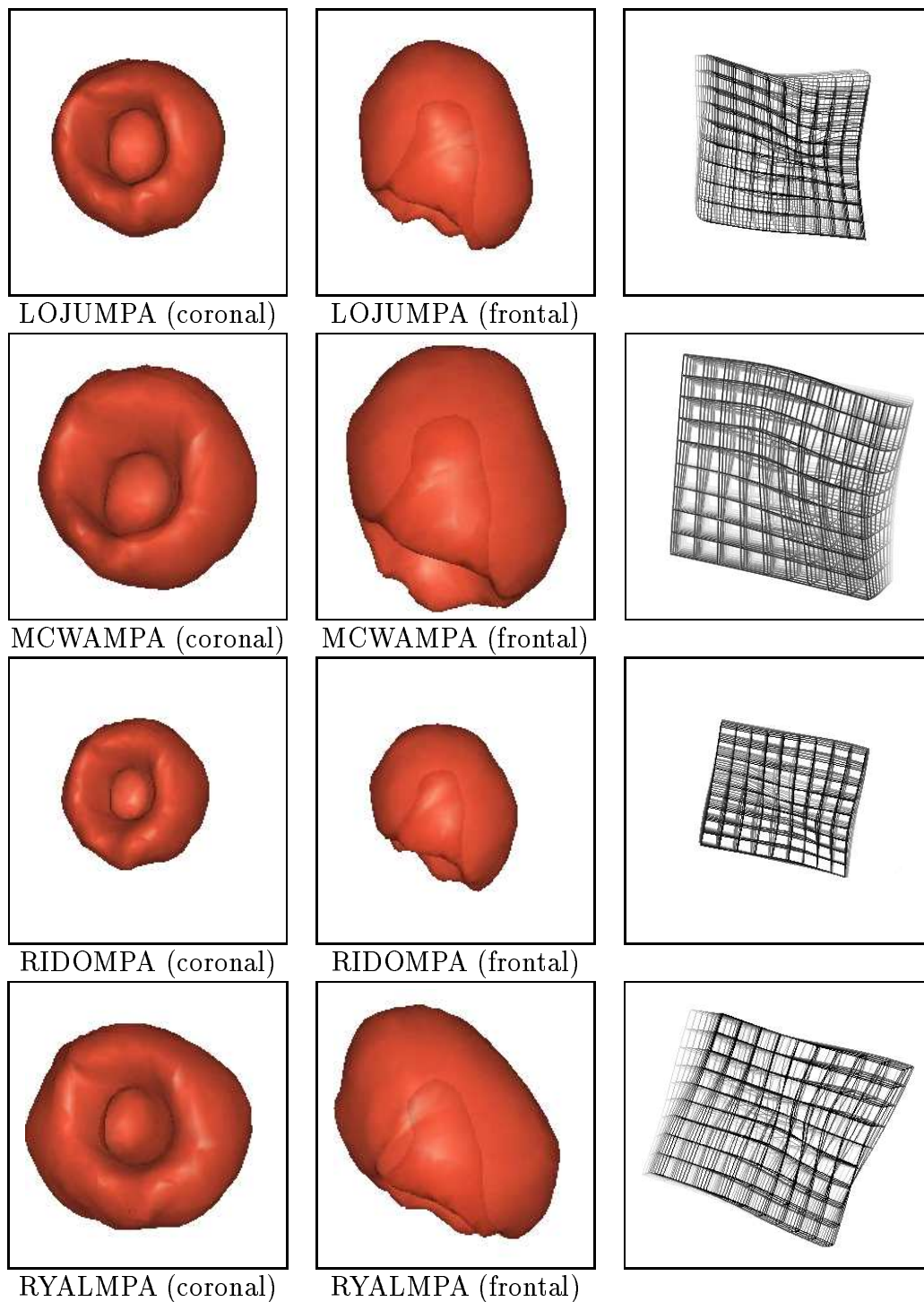


Figure 23: The closed surface of the template deformed to define the boundary of the left ventricle of 4 different hearts, left on a coronal projection and middle on a frontal projection. The surfaces are represented at the same scale, which allow to appreciate the differences in sizes and shapes. On the right, a regular grid is deformed by the alignment transformation.

References

- [1] P. Besl and N. McKay. A Method for Registration of 3D Shapes. *IEEE Transactions on Pattern Analysis and Machine Intelligence*, 14:239–256, February 1992.
- [2] J.C. Cauvin, J.Y. Boire, J.C. Maublant, J.M. Bonny, M. Zanca, and A. Veyre. Automated detection of the left ventricular myocardium long axis and center in Thallium-201 single photon emission computed tomography. *European Journal of Nuclear Medicine*, 19:1032–1037, 1992.
- [3] J. Declerck, G. Subsol, J.-P. Thirion, and N. Ayache. Automatic Retrieval of Anatomical Structures in 3D Medical Images. In *Computer Vision, Virtual Reality and Robotics in Medicine*, volume 905 of *Lecture Notes in Computer Science*, pages 153–162. Springer-Verlag, April 1995. (Also INRIA Research Report # 2485).
- [4] J. Feldmar and N. Ayache. Rigid, Affine and Locally Affine Registration of Free-Form Surfaces. *International Journal of Computer Vision*, In press. (Also INRIA Research Report # 2220).
- [5] E. Garcia, J. Maddahi, D. Berman, and A. Waxman. Space/time quantitation of Thallium-201 myocardial scintigraphy. *Journal of Nuclear Medicine*, 22:309–317, 1981.
- [6] E. Garcia, K.V. Van Train, and J. Maddahi. Quantification of rotational Thallium-201 myocardial tomography. *Journal of Nuclear Medicine*, 26:17–26, 1985.
- [7] G. Germano, P.B. Kavanagh, and H.T. Su. Automatic Reorientation of three-dimensional transaxial myocardial perfusion SPECT images. *Journal of Nuclear Medicine*, 36:1107–1114, 1995.
- [8] M.L. Goris, S. Boudier, and P.A. Briandet. Interrogation and display of single photon emission tomography data as inherently volume data. *American Journal of Physiologic Imaging*, 1:168–180, 1986.
- [9] M.L. Goris, S. Boudier, and P.A. Briandet. Two-dimensional mapping of three-dimensional SPECT data: a preliminary step to the quantitation of Thallium myocardial perfusion single photon emission tomography. *American Journal of Physiologic Imaging*, 2:176–180, 1986.
- [10] M.L. Goris, J. Sue, and M.A. Johnson. A principled approach to the "circumferential" method for Thallium myocardial perfusion scintigraphy quantitation. In *Noninvasive assessment of the cardiovascular system: diagnostic principle and techniques*. Edward P. Diethrich, John Wright, PSG, Inc., 1982.
- [11] A.S. Houston, P.M. Kemp, and M.A. MacLeod. A method for assessing the significance of abnormalities in HMPAO brain SPECT images. *Journal of Nuclear Medicine*, 35:239–244, 1994.

- [12] J. Maddahi, K. Van Train, and F. Pringent. Quantitative single photon emission computed Thallium-201 tomography for detection and localization of coronary artery disease: optimization and prospective validation of new technique. *Journal of Am Coll Cardiol*, 14:1689–1699, 1989.
- [13] J.J. Mahmarian, T.M. Boyce, and R.K. Goldberg. Quantitative exercise Thallium-201 single photon emission computed tomography for the enhanced diagnosis of ischemic heart disease. *Journal of Am Coll Cardiol*, 15:318–329, 1990.
- [14] O. Monga, R. Deriche, and J.M. Rocchisani. 3D edge detection using recursive filtering: application to scanner images. *Computer Vision Graphics and Image Processing*, January 1991.
- [15] R. Mullick and N.F. Ezquerra. 3D Visualization of pose determination: application to SPECT imaging. In *SPIE Second Conference on Visualization in Biomedical Computing*, volume 1808, pages 445–452. Chapel Hill, NC, October 1992.
- [16] R. Mullick and N.F. Ezquerra. Automatic Determination of LV Orientation from SPECT data. *IEEE Transactions on Medical Imaging*, 14:88–99, March 1995.
- [17] C. Perault, H. Wampach, and J.C. Liehn. Three-dimensional SPECT myocardial Rest-Stress subtraction images after automated registration and normalization. In Kluwer Academic Publisher, editor, *Proceedings of Information Processing and Medical Imaging*, volume 3, pages 391–392, June 1995.
- [18] J.-J. Risler. *Méthodes Mathématiques pour la CAO*. Masson, 1991.
- [19] P.J. Slomka, G.A. Hurwitz, J. Stephenson, and T. Craddock. Automated alignment and sizing of myocardial Stress and Rest scans to three-dimensional normal templates using an image registration algorithm. *Journal of Nuclear Medicine*, 36:1115–1122, 1995.
- [20] S.C. Strother, J.R. Anderson, K.A. Schaper, J.J. Sidtis, J.S. Liow, R.P. Woods, and D.A. Rottenberg. Principal Component Analysis and the Scaled Subprofile Model Compared to Intersubject Averaging and Statistical Parametric Mapping: I. "Functional Connectivity" of the Human Motor System Studied with O-15 Water PET. *Journal of Cerebral Blood Flow and Metabolism*, 15:738–753, 1995.
- [21] J.-P. Thirion. Fast Non-rigid Matching of 3D Medical Images. Technical Report RR 2547, INRIA, May 1995.
- [22] K.F. Van Train, D.A. Berman, and E. Garcia. Quantitative analysis of stress Thallium-201 myocardial scintigrams: a multicenter trial. *Journal of Nuclear Medicine*, 27:17–25, 1986.
- [23] K.F. Van Train, E. Garcia, and J. Maddahi. Improved quantitation of stress/redistribution Tl-201 scintigrams and evaluation of normal limits. In *IEEE transactions on Computers in Cardiology*, 1982.

- [24] K.F. Van Train, J. Meddahi, and D.A. Berman. Quantitative analysis of tomographic stress Thallium-201 myocardial scintigrams: a multicenter trial. *Journal of Nuclear Medicine*, 31:1168–1179, 1990.
- [25] A. Venot, J.C. Liehn, J.F. Lebruchec, and J.C. Roucayrol. Automated Comparison of Scintigraphic Images. *Journal of Nuclear Medicine*, 27:1337–1342, 1987.
- [26] R.A. Vogel. Quantitative aspects of myocardial perfusion imaging. *Seminars in Nuclear Medicine*, 10:146–155, 1980.
- [27] R.P. Woods, J.C. Mazziotta, and S.R. Cherry. MRI-PET registration with automated algorithm. *Journal of Computer Assisted Tomography*, 17:536–546, 1993.
- [28] Z. Zhang. Iterative point matching for registration of free-form curves and surfaces. *International Journal of Computer Vision*, 13(2):119–152, December 1994. Also INRIA Research Report #1658.



Unité de recherche INRIA Lorraine, Technopôle de Nancy-Brabois, Campus scientifique,
615 rue du Jardin Botanique, BP 101, 54600 VILLERS LÈS NANCY
Unité de recherche INRIA Rennes, Irisa, Campus universitaire de Beaulieu, 35042 RENNES Cedex
Unité de recherche INRIA Rhône-Alpes, 46 avenue Félix Viallet, 38031 GRENOBLE Cedex 1
Unité de recherche INRIA Rocquencourt, Domaine de Voluceau, Rocquencourt, BP 105, 78153 LE CHESNAY Cedex
Unité de recherche INRIA Sophia-Antipolis, 2004 route des Lucioles, BP 93, 06902 SOPHIA-ANTIPOLIS Cedex

Éditeur
INRIA, Domaine de Voluceau, Rocquencourt, BP 105, 78153 LE CHESNAY Cedex (France)
ISSN 0249-6399